
An accuracy study of mesh refinement on mapped grids

D. Calhoun and R. J. LeVeque, October, 2003

University of Washington Dept. of Applied Mathematics Seattle, WA, 98195

Summary. We test a high-resolution wave-propagation algorithm for hyperbolic conservation laws on mapped quadrilateral and hexahedral grids in the context of adaptive mesh refinement. We discuss some of the issues related to using non-Cartesian grids with AMR and study a test problem in which a grid refinement interface is fixed in space on a highly skewed portion of a mapped grid. Smooth and shock-wave solutions to the Euler equations are used to investigate the possibility that spurious reflections or other numerical errors might be generated at a grid interface.

Key words: gas dynamics, finite-volume, finite-difference, Cartesian grid, mapped grids, computational fluid dynamics, adaptive mesh refinement

1 Introduction

We study one approach to solving partial differential equations on a mapped grid in the context of AMR, using the finite volume wave-propagation algorithm described in [8] and [9] in two dimensions and in [6] in three dimensions. The application of this method to quadrilateral grids in two dimensions is discussed in [9] and recently we have implemented an extension to hexahedral grids in three dimensions. A logically rectangular computational grid is mapped to physical space via a mapping function that is applied to each corner of a grid cell. In two dimensions these corners can be connected by straight lines to obtain quadrilateral cells. In three dimensions the four corners on each face will typically not be co-planar but can be connected by ruled surfaces to obtain hexahedral physical cells. The wave-propagation algorithm is based on solving Riemann problems normal to the cell faces to obtain propagating waves. Limiters are applied to these waves and the limited waves used in “second-order” correction terms to obtain a high-resolution method.

These algorithms have been implemented with AMR in the style of Berger-Oligier and Berger-Collela [2, 3, 5] in the AMRCLAW software package as part of CLAWPACK [4, 7]. When this algorithm is applied to mapped grids, we refine grid cells by relying on an underlying smooth mapping function that tells us how to subdivide a coarse mesh cell. That is, the “midpoint” of two neighboring corners of

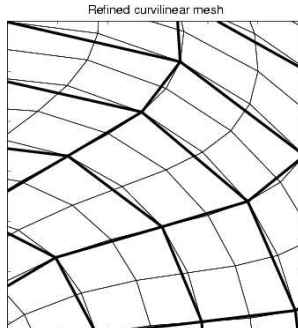


Fig. 1. Refined mapped grid shows the potential misalignment between coarse and fine grid cells. The coarse mesh is represented by thick lines and corresponding fine mesh is shown in thin lines.

a coarse cell is defined as the point along the curve, defined by our smooth mapping, passing through those two points. This eliminates the need to construct a smooth mapping through coarse grid points, as is done, for example, in the method developed in [1, 10]. Our strategy has the advantage of simplicity, particularly when extending the method to three dimensions. The disadvantage of this strategy, however, is that underlying refined cells are not necessarily contained in their corresponding coarse cell. See Figure 1 for an illustration of this. This is a potential source of error and part of our goal here is to investigate whether this simpler approach is sufficient or generates unacceptable errors.

Since refined cells are not necessarily contained within their coarse cell, one might suspect that volumes are not preserved and interpolation between coarse and fine grids might not be conservative. We address this issue by using the capacity function formulation of the equations as discussed in [8], [9]. The capacity κ_{ij} of a grid cell plays the role of a discrete Jacobian and is the ratio of the physical volume of a mesh cell to the volume in computational space. We use this in our fine to coarse interpolation. For example, in two-dimensions, a coarse value Q_{ij} is determined from its four fine grid values Q_{ij}^k , $k = 1, \dots, 4$ using the formula

$$Q_{ij} = \frac{\sum_{k=1}^4 \kappa_{ij}^k Q_{ij}^k}{4\kappa_{ij}}. \quad (1)$$

This formula will assure that the conserved quantities are properly conserved between coarse and fine grids in spite of the fact that refined cells are not exactly aligned with their coarse grid cells. We may lose accuracy, however, unless

$$\kappa_{ij} = \frac{1}{4} \sum_{k=1}^4 \kappa_{ij}^k. \quad (2)$$

This is satisfied with the refinement strategy of [1, 10], but is not satisfied with our approach. Consequently, constant states are not exactly preserved between coarse and fine grids. We show that results look promising even though (2) is not strictly satisfied.

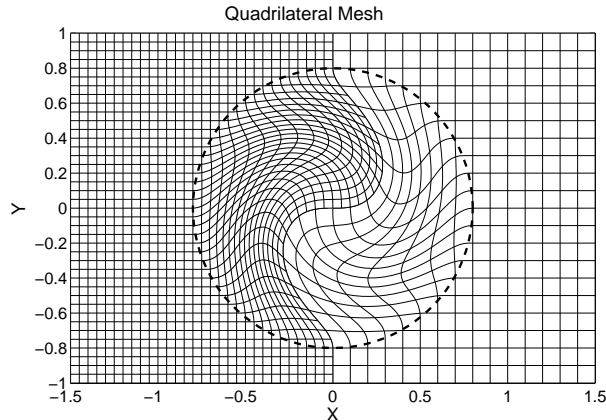


Fig. 2. Mapped partially refined grid used for two dimensional numerical studies. This plot shows every fourth grid line on a mesh with 120 coarse grid points in the x -direction. The circular region encloses the mapped area.

At coarse-fine boundaries, we use the conservation fix-up described in [5]. In this fix-up, we must solve Riemann problems between ghost cells of the fine grid, and the coarse cells that border the fine grid. On a quadrilateral or hexahedral mesh in which the fine grid cell edges do not line up with coarse cell edges, we use the coarse grid cell edges to determine the rotation angle necessary to define the Riemann problem required in the fix-up step.

2 Numerical results

Our main goal is to provide insight into the accuracy that can be expected when using the wave-propagation algorithm on a mapped Cartesian grid in the presence of a grid refinement interface. Normally in AMR the fine grids are constantly adapted to follow strong solution features such as shock waves. However, in complicated flow problems there are other nontrivial features such as smooth profiles or weaker shocks that are not always covered by refinement but rather move across the fine-coarse interface. To study the effect of such an interface on the solution we use a test problem in which the region of refinement is *fixed* and a solution feature moves across the interface. In order to obtain quantitative comparisons we choose a simple situation in which the true solution is a one-dimensional plane wave.

We show results for test problems on a quadrilateral grid of the type shown in Figure 2 and the hexahedral generalization shown in Figure 8. In each case the grid is Cartesian near the edges of the domain, but a circular region of radius $R = 0.8$ about the origin is rotated by the smooth grid mapping that in two dimensions takes the form

$$\begin{aligned} X(\xi, \eta) &= \cos(\alpha(r)\theta)\xi + \sin(\alpha(r)\theta)\eta \\ Y(\xi, \eta) &= -\sin(\alpha(r)\theta)\xi + \cos(\alpha(r)\theta)\eta \end{aligned} \quad (3)$$

where the parameter θ defines the maximum skewness of the grid, and $\alpha(r)$ allows us to smoothly connect the uniform region of the grid with the rotated region. For our problems, we have defined $\alpha(r)$ as

$$\alpha(r) = \begin{cases} (1 + \cos(\pi r/R))/2 & r < R \\ 0 & \text{otherwise} \end{cases} \quad (4)$$

where r is the distance to the grid origin $(0, 0)$. Figure 2 shows grids corresponding to values $\theta = \pi/2$, the value used in all tests shown here. The advantages of this grid are that (1) the boundaries are straight, thereby eliminating any numerical issues that might arise at curved boundaries, (2) we can adjust the skewness of the grid with a single parameter and test how numerical errors are influenced by the skewness of the grid, and finally, (3) the initial values are concentrated in a region in which the pointwise values of the initial data and the cell averaged values are close, thereby eliminating the need to compute cell averages in cells which have been distorted by the grid mapping.

We solve the Euler equations with two sets of initial data, and in all both examples, report on the computed density. In the first example, we simulate a planar Mach 2 shock wave, and in the second example, we simulate a smooth acoustic wave with initial data

$$\begin{aligned} \rho_0(x, y) &= 1 + 0.25 \exp(-5(x + 1.5)^2) \\ p_0(x, y) &= \rho_0^\gamma, \\ u_0(x, y) &= \frac{2}{\gamma - 1} \left(\sqrt{\gamma \rho_0^{\gamma-1}} - \sqrt{\gamma} \right) + 2. \end{aligned} \quad (5)$$

This data is chosen so that the wave is a simple wave that remains smooth over the time interval considered. In each case the solution feature is initially on the Cartesian portion of the grid and passes through the rotationally skewed portion. The true solution is purely one-dimensional. The computed density on the two- or three-dimensional mapped grid is compared with a fine grid or exact solution, and with a numerical solution to the one-dimensional equations computed using the wave-propagation algorithm on a grid with the same number of grid points as are used in the x -direction on the multidimensional grid. If the multidimensional grid were purely Cartesian ($\theta = 0$ in (3)) then the multi-dimensional results would match the one-dimensional results. On the skewed grid we do not expect the results to be as good and so this gives some basis for examining the effect of the grid mapping.

2.1 Two-dimensional results

In Figure 3 we show the two-dimensional results for the shock-wave test problem on a single (unrefined) grid with $\theta = \pi/2$. In spite of the skewed grid the contour lines show that the numerical solution is essentially one-dimensional. The left plot in Figure 5 shows a scatter plot of the density in all grid cells, plotted against the x -coordinate of the cell center. This is compared with the exact solution based on the computed shock speed.

We now turn to testing the behavior of the solution when the feature passes through a fine-coarse grid interface. We force a static refinement in which the left portion of the computational domain is refined by a factor of 2 relative to the right

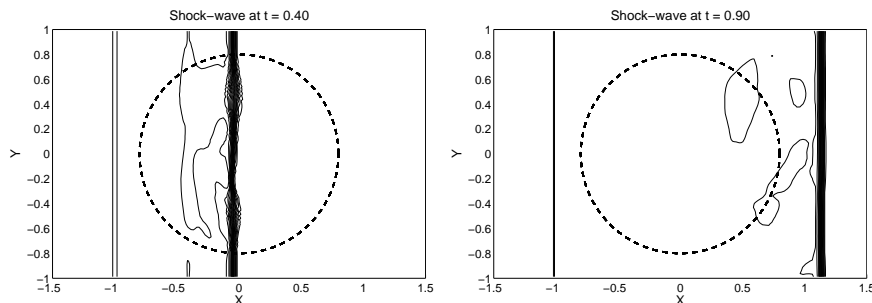


Fig. 3. Contours of the solution to shock-wave problem on a single grid at times $t = 0.4$ and $t = 0.9$. The dashed circle encloses the mapped region. The contour levels are $0.95 : 0.1 : 2.95$. The grid is 120 cells in x -direction ($dx = 0.025$).

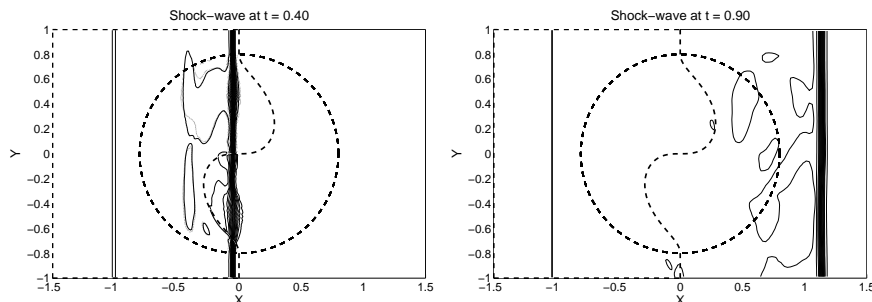


Fig. 4. Contours of the solution to shock-wave problem on a partially refined grid at times $t = 0.4$ and $t = 0.9$. The dashed circle encloses the mapped region, and the additional dashed center-line is the right edge of the refined region. The contour levels are $0.95 : 0.1 : 2.95$. The coarse grid resolution for these plots is 120 cells in x -direction ($dx = 0.025$).

portion, as shown in Figure 2. Note that the refinement boundary is chosen to be in the region of maximum grid deformation. In this region the fine and coarse grid cells do not exactly match up, as was shown in Figure 1, and a concern is that the interface will lead to the generation of spurious reflections or other numerical noise at the interface. Of course this can be a problem at a refinement interface even on a purely Cartesian grid, but the grid deformation and mismatch of cells heightens the concern.

Our results indicate that the wave-propagation algorithm appears to behave well in this regard, at least on the test problems used here. The two plots in Figure 4 show contour lines of the shock wave in the middle of the mapped region, and again once it has completely left the mapped and refined region. Figure 5 shows scatter plots of the solution computed on a single coarse grid (left plot) and a partially refined grid

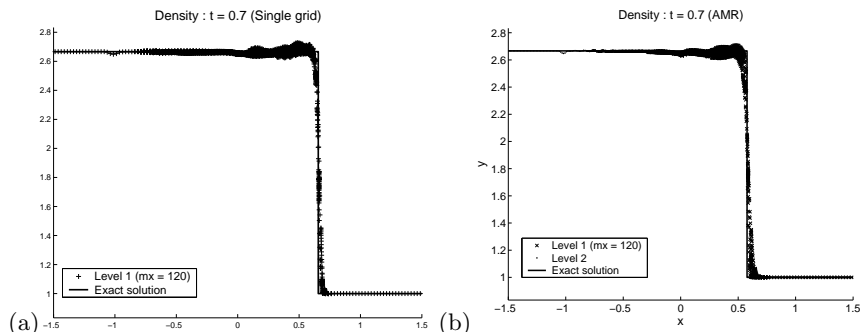


Fig. 5. Scatter plot of shock-wave solution computed on (a) a single grid and (b) after is passed through a coarse-fine interface on a partially refined grid.

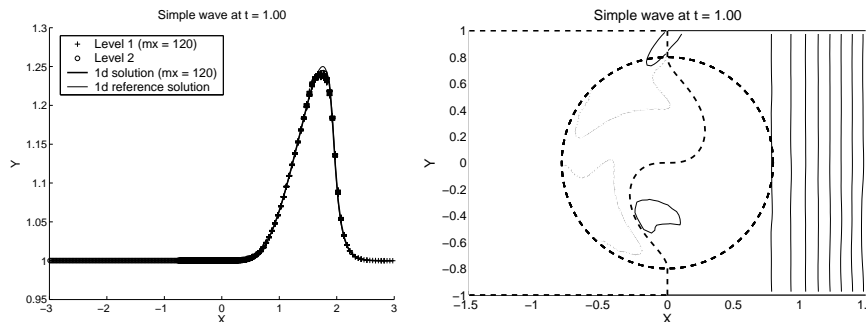


Fig. 6. Scatter plot and contour plot of simple wave solution. Both plots show the solution computed on a grid in which the left half was refined. Coarse grid resolution is 120 cells in the x -direction. ($dx = 0.05$).

(right plot). For comparison, the exact solution, based on the computed shock speed is also shown on both plots. What we hope to observe, is that the results on the partially refined grid are no worse than what was obtained on the unrefined coarse grid. In fact we do observe this, indicating that the existence of a refined patch does not introduce substantial errors at the grid interface. We also don't expect to see substantially better results on the partially refined grid, since the shock has already left the refined region by time $t = 0.7$.

Figure 6 shows similar plots for the smooth test problem with data (5). Figure 7 shows the results of a grid refinement study on this smooth test problem. The upper curve shows the L_1 norm of the error found on a sequence of unrefined grids, indexed by the number of grid points in the x -direction. The lower curve shows corresponding results for a sequence of partially-refined grids, indexed by the number of grid points in x on the coarse grid. These results show that the method remains second order accurate in spite of the refinement boundary. The error is no larger on the partially-

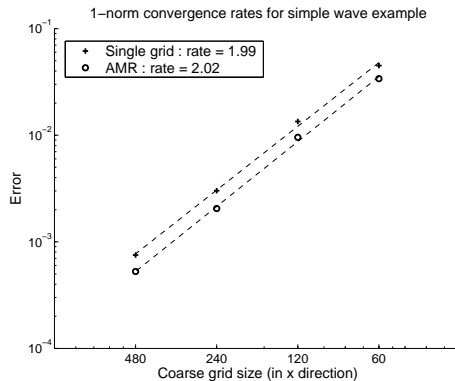


Fig. 7. Convergence results for simple wave solution. Two curves show the single grid errors (top curve) and the errors on a mesh in which the left half was refined (bottom curve).

refined grid than on the single grid, and in fact is slightly smaller since the solution was initialized on the finer grid. This indicates that excessive errors are not being introduced at the refinement boundary.

2.2 Three-dimensional results

Tests have been performed for the three-dimensional hexahedral generalization of these test problems, with similar results. The grid used for these simulations is the three-dimensional analog of the two-dimensional grid used above. In three-dimensions, we rotate a spherical region of radius $R = 0.8$, centered at the origin, by an angle $\alpha(r)\theta$ about a vector v . For the following simulations, we set $\theta = \pi/2$ and $v = (1, 1, 1)$. The function $\alpha(r)$ is defined as in (4). The three dimensional grid is shown in Figure 8.

To determine necessary geometric quantities for each mesh cell, we approximate the hexahedral mesh by a trilinear map

$$T(\xi, \eta, \zeta) = a_{000} + a_{100}\xi + a_{010}\eta + a_{001}\zeta + a_{110}\xi\eta + a_{101}\xi\zeta + a_{011}\eta\zeta + a_{111}\xi\eta\zeta \quad (6)$$

where $0 \leq \xi, \eta, \zeta \leq 1$. The coefficients $a_{lmn} \in \mathcal{R}^3$ are computed from the locations of the physical corners of the mesh cell. This approximation is the natural extension of two dimensional bilinear quadrilateral mesh cells to three dimensions. Using this approximation, we compute a set of normal and tangential vectors at the midpoint of each face, a surface area for each face, and the volume of the approximated mesh cell. These quantities are then used in the Riemann problems and in update formulas in a manner analogous to the what we do in two-dimensions.

To test our code, we use the same simple wave and Mach 2 shock examples that we discussed in our two dimensional test problems. In Figure 9, we show a scatter plot and a contour plot, on a $z = 0$ slice of data for the smooth-wave computed on

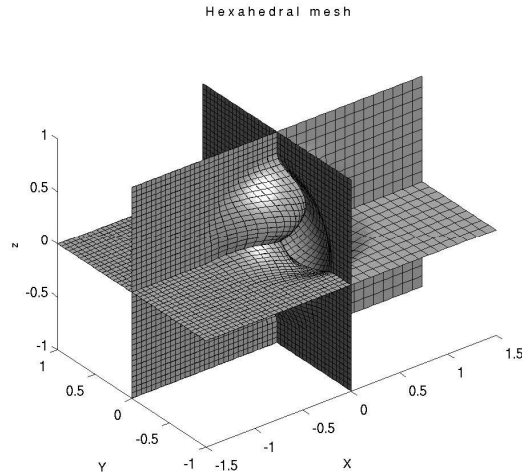


Fig. 8. Hexahedral mesh used for three-dimensional simulations. The center region has been rotated about the vector $v = (1, 1, 1)$ by a skewness factor of $\theta = \pi/2$. This plot shows every other grid line in a mesh with 60 coarse grid cells in the x -direction ($dx = 0.05$).

the partially refined grid. In Figure 10 we show the results of the Mach 2 shock-wave, on a ($z = 0$) slice, at two different times, and in Figure 11, we show a scatter plot of the same shock-wave results. In both examples, the results are no worse than results computed on a single grid at the coarse grid resolution, indicating that the introduction of a refined grid and a coarse/fine boundary does not cause spurious waves or reflections. The accuracy does not appear to be as good as on the two dimensional grid, but this is due in part to the fact that we are computing the three dimensional solution on a grid with half the resolution as was used in the two-dimensional example.

3 Conclusions

We have proposed a simple test problem to study the effect of introducing a mesh refinement boundary when solving conservation laws on a mapped grid. A static refinement interface is introduced in a highly skewed region of the grid and both a shock wave and a smooth simple wave are passed through this interface to test for spurious reflections or loss of accuracy. We have tested the wave-propagation algorithm in two and three dimensions and have observed results that are better than what is obtained on an unrefined grid. This is encouraging since a refinement strategy is used in which the grid cells are not perfectly aligned between coarse and fine cells, which could potentially generate significant errors at the interface.

Acknowledgment. This work was supported in part by DOE grant DE-FC02-01ER25474 and NSF grant DMS-0106511.

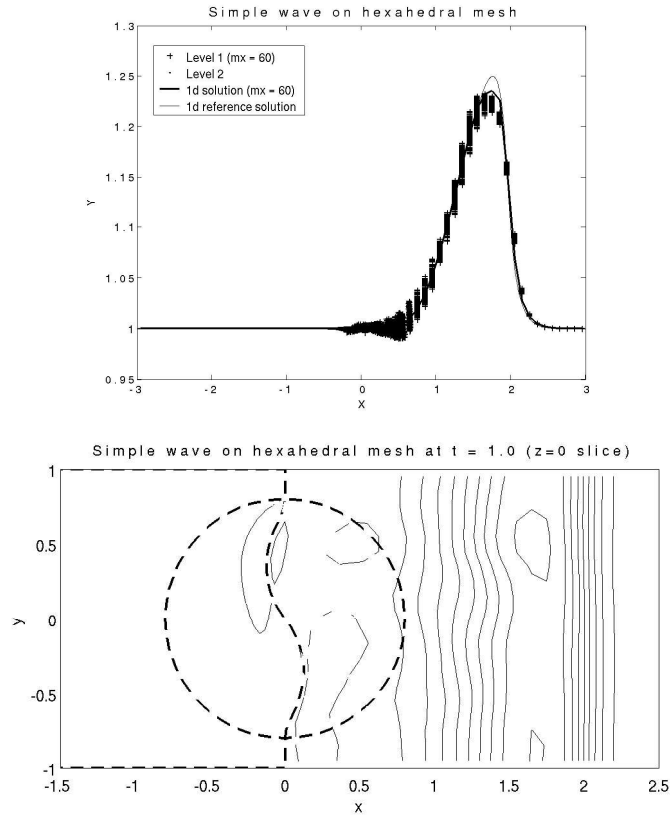


Fig. 9. Solution to simple wave problem computed on a partially refined hexahedral grid. The coarse grid resolution is 60 grid cells in the x -direction ($dx = 0.05$).

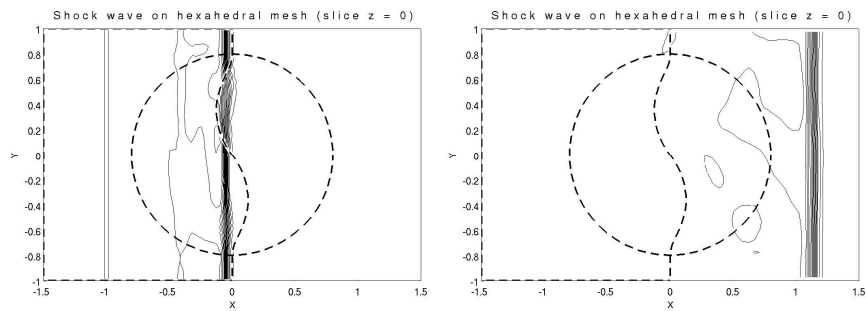


Fig. 10. Solution to shock-wave problem computed on a partially refined hexahedral grid. The coarse grid resolution is 60 grid cells in the x -direction ($dx = 0.05$).

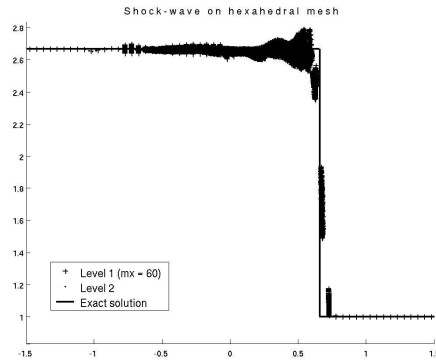


Fig. 11. Scatter plot of density in the shock-wave problem computed on a hexahedral mapped grid. The coarse grid resolution is 60 grids in the x -direction ($dx = 0.025$).

References

1. J. B. Bell, P. Colella, J. Trangenstein, and M. Welcome. Adaptive mesh refinement on moving quadrilateral grids. Technical report, Lawrence Livermore National Laboratory, April 1989.
2. M. Berger and J. Olinger. Adaptive mesh refinement for hyperbolic partial differential equations. *J. Comput. Phys.*, 53:484–512, 1984.
3. M. J. Berger and P. Colella. Local adaptive mesh refinement for shock hydrodynamics. *J. Comput. Phys.*, 82:64–84, 1989.
4. M. J. Berger and R. J. LeVeque. AMRCLAW software. Available on the Web at the URL <http://www.amath.washington.edu/~claw/>.
5. M. J. Berger and R. J. LeVeque. Adaptive mesh refinement using wave propagation algorithms for hyperbolic systems. *SIAM J. Num. Anal.*, 35(6):2298–2316, 1998.
6. J. O. Langseth and R. J. LeVeque. A wave-propagation method for three-dimensional hyperbolic conservation laws. *J. Comput. Phys.*, 165:126–166, 2000.
7. R. J. LeVeque. CLAWPACK software. Available on the Web at the URL <http://www.amath.washington.edu/~claw/>.
8. R. J. LeVeque. Wave propagation algorithms for multidimensional hyperbolic systems. *J. Comput. Phys.*, 131:327–353, 1997.
9. R. J. LeVeque. *Finite volume methods for Hyperbolic problems*. Cambridge University Press, 2002.
10. E. Steinhilber, D. Modiano, and P. Colella. Computations of unsteady viscous compressible flows using adaptive mesh refinement in curvilinear body-fitted grid systems. Technical Report NASA Technical Memorandum 106704, NASA, 1994.